ELSEVIER

Materials Science and Engineering A 487 (2008) 128–136

MATERIALS SCIENCE & ENGINEERING A

www.elsevier.com/locate/msea

Simulation of competitive Cu precipitation in steel during non-isothermal aging

J.B. Yang [1], T. Yamashita [b], N. Sano [c], M. Enomoto [a,*]

[a] *Department of Materials Science and Engineering, Ibaraki University, Ibaraki 316-8511, Japan*
[b] *Steel Research Laboratories, JFE Steel Corporation, Japan*
[c] *The Corporate R&D Laboratories, Sumitomo Metal Industries, Ltd., Japan*

Received 15 April 2007; received in revised form 29 September 2007; accepted 6 October 2007

Abstract

A numerical model has been developed to simulate Cu precipitation in dilute bcc Fe–Cu alloys during non-isothermal aging taking into account competitive nucleation at grain boundaries, dislocations and in the matrix, and structural transformation of Cu particles that occurs during growth. The temporal evolution of number density, mean particle size and size distribution during continuous cooling is simulated and is compared with experimental observations under transmission electron microscope and three-dimensional atom probe field ion microscope. With decreasing temperature the growth and coarsening rates diminishes rapidly whereas nucleation continues to occur down to lower temperatures due to the decrease in the activation energy of nucleation and thus, distributions of fine particles can be obtained relatively easily after cooling. Precipitation and dissolution during continuous heating are simulated and are compared with experimental observations in the literature.

Keywords: Nucleation; Growth; CCT; Solute cluster; Cu bearing steel

1. Introduction

Cu precipitation in steel has attracted considerable attention for more than half a century because it causes irradiation embrittlement in structural steels of nuclear reactor. Besides it arouses interest among people for various reasons; the combination of strength and ductility is improved in low carbon tempered martensitic steels: bake-hardenability can be improved in pre-strained ferritic steels. It has also attracted attention with respect to recycling of scrap steels.

Several authors attempted modeling of Cu precipitation in iron alloys during thermal aging and under irradiation. They include modified Langer–Schwartz (MLS) model [1,2], N-model [1,3,4], Monte Carlo simulation [5–7] and cluster dynamics [8]. The present authors employed N-model to simulate precipitation of Cu particles in thermal aging in regard to steel microstructure, more specifically taking into account competition between homogeneous and heterogeneous nucleation sites, e.g. dislocations and lath boundaries [4]. In these simulations the competitive precipitation was treated introducing solute-depleted zones for heterogeneous nucleation sites in which mass balance of solute was treated independently from the rest of the system.

Industrial processes customarily consist of not only isothermal, but also non-isothermal heat treatment. In fact, N-model was employed to simulate non-isothermal precipitation in Al alloys [9,10]. Accordingly, a model has been developed to simulate Cu precipitation during continuous cooling and heating in steel that has more than one type of heterogeneous nucleation sites. The phase transformation of precipitates is treated phenomenologically.

2. Simulation method

2.1. N-model of competitive nucleation

The system is divided into zones associated with the type of nucleation sites as shown in Fig. 1, where Ω_λ is the volume fraction of the λth zone ($\lambda = 1$, 2 and 3 for matrix, dislocations and grain boundaries), ω_λ is the volume fraction of particles in that zone and c_0, c_p and $\bar{c}_\lambda$ are the Cu concentration in the

* Corresponding author. Tel.: +81 294 38 5058; fax: +81 294 38 5226.
E-mail address: enomotom@mx.ibaraki.ac.jp (M. Enomoto).
[1] Now at: The Oarai Branch, Institute for Materials Research, Tohoku University, Oarai, Ibaraki 311-1313, Japan.

0921-5093/$ – see front matter © 2007 Elsevier B.V. All rights reserved.
doi:10.1016/j.msea.2007.10.068

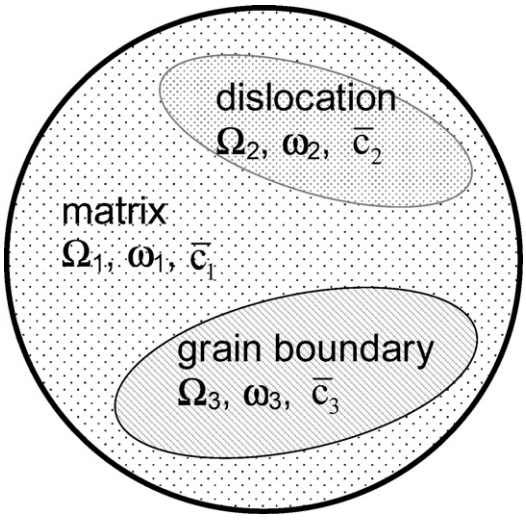

Fig. 1. Nucleation zones associated with heterogeneous nucleation sites, e.g. dislocation and grain boundary. The mean solute concentration differs from each other.

bulk, in the particles and the mean concentration in the region excluding precipitates in the λth zone, respectively. The total particle number N, the particle number N_λ and mean particle radius $\bar{R}_\lambda$ in the λth zone and $\bar{c}_\lambda$ are calculated at very fine time steps. The mean concentration in the matrix of each zone is updated at every time steps, using the mass balance equations [3,4]

$$c_0\Omega_\lambda = \bar{c}_\lambda(\Omega_\lambda - \omega_\lambda) + c_p\omega_\lambda \quad \text{for } \lambda = 1, 2 \text{ and } 3 \tag{1}$$

Fig. 2 shows a path of cooling and heating envisaged in this study. bcc and fcc Cu particles are nucleated at grain boundaries, dislocations and in the matrix during the heat treatment. According to the classical nucleation theory [11], the time dependent nucleation rate is given by

$$J* = N_v\beta * Z \exp\left(-\frac{\Delta G*}{kT}\right) \exp\left(-\frac{\tau}{t}\right) \tag{2}$$

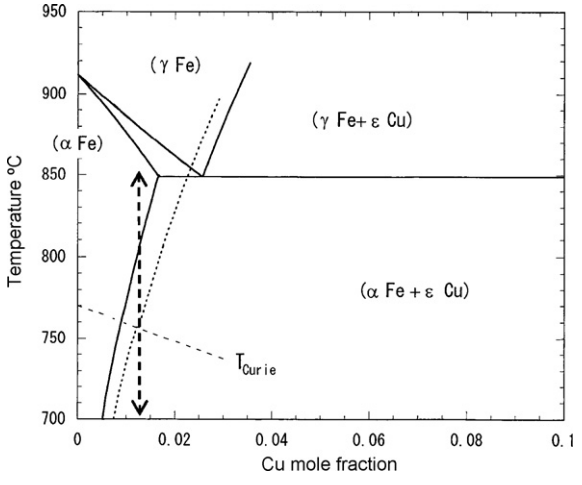

Fig. 2. Fe corner of Fe–Cu binary phase diagram [31]. A dotted curve is the miscibility gap of the bcc solid solution. A dashed curve is the Curie temperature. A vertical arrow shows cooling and heating of a Fe–1.5 wt% Cu alloy.

where N_v, β^*, Z, ΔG^* and τ are, respectively, the number of potential nucleation sites, frequency factor, Zeldovich non-equilibrium factor, activation energy of nucleation and incubation time. All these, but N_v are calculated assuming a spherical nucleus in the matrix and a double spherical cap nucleus on grain boundaries. They are given by

$$\beta^* = \frac{16\pi\sigma^2 D\bar{c}}{a^4(\Delta G_V)^2}, \quad Z = \frac{v_a(\Delta G_V)^2}{8\pi(kT\sigma^3)^{1/2}}, \quad \Delta G^* = \frac{16\pi\sigma^3}{3(\Delta G_V)^2},$$

$$\text{and} \quad \tau = \frac{8kT\sigma a^4}{v_a^2(\Delta G_V)^2 Dc} \tag{3}$$

for nucleation in the matrix, where a, σ, D and v_a are the lattice parameter, nucleus/matrix interfacial energy, solute diffusivity, volume of an atom in the nucleus and kT has its usual meaning. ΔG_V is the volume free energy change attending nucleation and is calculated from the equation

$$\Delta G_V = \frac{kT}{v_a} \ln \frac{\bar{c}}{c_e} \tag{4}$$

where c_e is the solubility of bcc or fcc Cu, which was calculated by Thermo-calc using the parameter values in the Scientific Group Thermodata Europe (SGTE) solution data base [12]. For nucleation on grain boundaries they are given by

$$\beta^*_{gb} = \beta^* L(\theta), \quad Z_{gb} = \frac{Z}{\sqrt{K(\theta)}}, \quad \Delta G^*_{gb} = \Delta G^* K(\theta),$$

$$\text{and} \quad \tau_{gb} = \tau\frac{K(\theta)}{L(\theta)} \tag{5}$$

where $K(\theta)$ and $L(\theta)$ are defined by

$$K(\theta) = \frac{(2+\cos\theta)(1-\cos\theta)^2}{4},$$

$$L(\theta) = 1 - \cos\theta \quad \text{and} \quad \cos\theta = \frac{\sigma_b}{2\sigma}$$

and θ is the contact angle of a nucleus with the grain boundary. The incubation time for continuous cooling (or heating) is calculated assuming that the additivity rule is valid, that is, from the equation

$$\sum_{i=1}\frac{\Delta t}{\tau_i} = \frac{\Delta t}{\tau_1} + \frac{\Delta t}{\tau_2} + \cdots + \frac{\Delta t}{\tau_n} = \frac{t}{\tau} \tag{6}$$

where τ_i is the incubation time of the ith time step.

For nucleation at dislocations it is reported that spherically shaped coherent precipitates, whose shear modulus is larger than that of the matrix, can be nucleated alongside a dislocation [13,14]. Indeed, the elastic constants of bcc Cu are somewhat greater than those of αFe [15,16]. Although direct experimental evidence is yet to be available, it is assumed that coherent bcc Cu clusters are nucleated at dislocations. One cannot, however, rule out the possibility that fcc Cu particles are nucleated at highly disordered sites, e.g. kinks and jogs of dislocations. The Larche's effective interfacial energy for coherent nucleation alongside a dislocation [14]

$$\sigma_d = \sigma - \frac{\mu b(1+\nu)}{9\pi(1-\nu)}|\varepsilon| \tag{7}$$

where b(=2.47 × 10^{-10} m) is the Burgers vector of the dislocation, μ(=81.6 GPa) is the shear modulus, ν(=0.293) is the Poisson's ratio and ε(∼0.03) [15,16] is the misfit strain of the particle in the matrix, is used for nuclei of bcc Cu on dislocations. In the calculation the nucleus/matrix interfacial energy is assumed to be 0.27 J/m^2 for bcc [17], whereas the interfacial energy of fcc ε-Cu is reported to be 0.52 J/m^2 [18].

For simulation of grain boundary precipitation one needs to incorporate the distribution of grain boundary character and energies. To the best of the authors' knowledge this has not been done. Here, we assume that all grain boundaries have a single energy $\sigma_b = 0.8$ J/m^2, the experimental value reported earlier for a bcc Fe-C alloy [19]. Boundaries are then wet for nucleation of bcc Cu. As shown later (Fig. 4b), a smaller number of coarse particles are observed at grain boundaries. Whereas bcc Cu could be nucleated at some boundaries of lower energy, fcc Cu particles are assumed to be nucleated on grain boundaries.

Precipitates occupy a progressively larger number of nucleation sites with time. The decrease in the number of unoccupied sites at grain boundaries per unit volume is given by

$$N_b = \frac{1}{a^2}(S_G - \pi \bar{R}_3^2 N_3) \tag{8}$$

where S_G is the grain boundary area per unit volume. It is equal to $S_G = 3.35/d$ if the matrix consists of tetrakaidecahedra of equal size [20], where d is the distance between square faces (d is taken to be a grain size in the later section). On the other hand, the decrease in the number of unoccupied nucleation sites at dislocations is written as [4]

$$N_d = \frac{1}{a^2}(\rho - 2\bar{R}_2 N_2) \tag{9}$$

where ρ is the dislocation density.

2.2. Pipe diffusion- and grain boundary diffusion-assisted growth of precipitates

Under the mean field approximation the growth rate of particles nucleated in each zone is calculated from the equation

$$v_{i,\lambda} = \frac{dR_{i,\lambda}}{dt} = \frac{\bar{c}_\lambda - c_R}{c_p - c_R}\frac{D}{R_{i,\lambda}} \tag{10}$$

where c_R is the Cu concentration at the particle/matrix and D is the diffusivity that rate-controls the growth of particles. $R_{i,\lambda}$ is the radius of particles at the ith time step in the λth zone. In other N-models newly formed nuclei were allocated to a predetermined size class, and the growth rates of particles were calculated at the edges of the size class [1,21]. In this model the growth rates of all particles are calculated in a straightforward manner. In principle the critical nucleus cannot grow because it is at (unstable) equilibrium with the matrix. It is assumed that the nucleus starts to grow when the radius becomes $R^* + \Delta R$ by thermal fluctuation, where ΔR satisfies the condition $\Delta G = \Delta G^* - kT/2$ [11,22]. Thus, the initial radius becomes

$$R = R^* + \Delta R \approx R^* + \sqrt{\frac{kT}{8\pi\sigma}} \tag{11}$$

The transport of solute is assisted by diffusion along the dislocation core and grain boundaries, the latter being established as collector plate mechanism [23]. For particles on grain boundaries the apparent diffusivity that controls nucleation and growth can be expressed approximately as $D \sim (D_b^2 D_v)^{1/3}$ at early and middle stages at which the overlap of diffusion fields within the boundaries is not significant, where D_b is the diffusion coefficient along grain boundaries and D_v, the volume diffusivity. For particles on dislocation the corresponding diffusivity is assumed to be $D \sim (D_p D_v^2)^{1/3}$, where D_p is the pipe diffusion coefficient. $D_v \sim 2D_{Fe} = 1.0 \times 10^{-4} \exp(-240{,}000/R_g T)$ m^2/s and $D_b\delta \sim 5.4 \times 10^{-14} \exp(-155{,}000/R_g T)$ m^2/s were taken from the compilation by Fridberg et al. [24], where δ is the boundary thickness and R_g is the gas constant. The activation energy of pipe diffusion D_p was calculated assuming that the ratio of the activation energy of pipe diffusion to that of volume diffusion is ∼0.73 [25]. It is well known that Cu particles undergo a structural transformation, following the sequence bcc → 9R → fcc when it grows to a few nm in diameter [26,27]. The change in solubility of Cu and particle/matrix interfacial energy accompanies the transformation. In view of the lack of data on twinned 9R structure it is assumed that the parameter values change from those of bcc to fcc Cu when the particle radius becomes 2.5 nm.

2.3. Expansion of solute-depleted zone

Fig. 3 shows a schematic illustration of the solute-depleted zone associated with grain boundaries (zone 3). In case that the thickness of the solute-depleted zone ℓ is not so large compared with the grain size the area of interface per unit volume is given approximately by

$$S_3 \approx 2\left(\frac{d - 2\ell}{d}\right)^2 S_G \tag{12}$$

where a factor 2 is due to the fact that interfaces are present on both sides of a boundary. On the other hand, the volume fraction

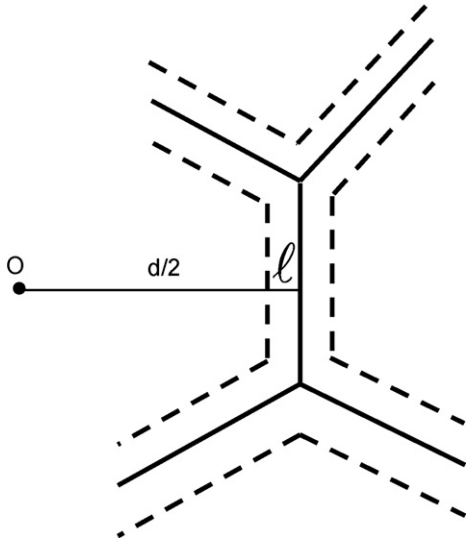

Fig. 3. Schematic illustration of solute-depleted zone of grain boundary (zone 3).

of zone 3 is given by

$$\Omega_3 \approx 1 - \left(\frac{d - 2\ell}{d}\right)^3 \tag{13}$$

It is assumed that at late stages the rate of expansion of the zone is controlled by the flux of Cu atoms into the zone from the matrix. It is expressed as

$$D\frac{\mathrm{d}c}{\mathrm{d}x}S_3 = DS_3\frac{\bar{c}_1 - \bar{c}_3}{\ell} \approx (c_0 - \bar{c}_3)\frac{\mathrm{d}\Omega_3}{\mathrm{d}t} \tag{14}$$

In the r.h.s. of the above equation c_0 is relevant because both the matrix and precipitates therein are taken into zone 3 as zone 1 is eaten away. Thus, from Eqs. (12) and (13) the increasing rate of the zone thickness is given by

$$\frac{\mathrm{d}\ell}{\mathrm{d}t} \approx \frac{\bar{c}_1 - \bar{c}_3}{c_0 - \bar{c}_3}\frac{D}{\ell} \tag{15}$$

where a factor 1.12 arising out of differentiation of Eq. (13) was omitted. A solute-depleted zone is developed around dislocations in a similar way. At sufficiently long times the radius of solute-depleted zone around dislocation (zone 2), denoted r_d, is given by

$$\frac{\mathrm{d}r_\mathrm{d}}{\mathrm{d}t} \approx \frac{\bar{c}_1 - \bar{c}_2}{c_0 - \bar{c}_2}\frac{D}{r_\mathrm{d}} \tag{16}$$

as has been described elsewhere [3,4].

3. Experimental procedure

Electrolytic iron and high-purity copper were vacuum induction melted. The alloy composition is shown in Table 1. A 50 kg ingot was hot rolled to a final thickness of 4 mm at 1200 °C and was air-cooled. During air-cooling the slab may undergo γ to α massive transformation. The hot-rolled slab was then solution treated at 830 °C for 10 min and cooled down to 200 °C at $L = 0.02$ and 0.1 °C/s, and was quenched. The specimens were observed under a transmission electron microscope (JEM-2010F) operated at 200 kV. Cu particles were observed in bright field under a defocused condition. A STEM-EDX analysis showed that they were indeed Cu particles. A substantial fraction of dislocations may have been annihilated during solution treatment and cooling. Thus, it was assumed that particles that grew to ~10 nm or larger were formed on dislocations. The mean radius and number density of particles on dislocations were evaluated from micrographs of ca. 10 areas, assuming that the specimen thickness was 100–300 nm. Fig. 4a shows a TEM

Table 1
Chemical composition of alloy (wt%)

Cu	1.5
C	0.001
Mn	0.01
Si	0.01
P	0.001
S	0.001
N	0.001

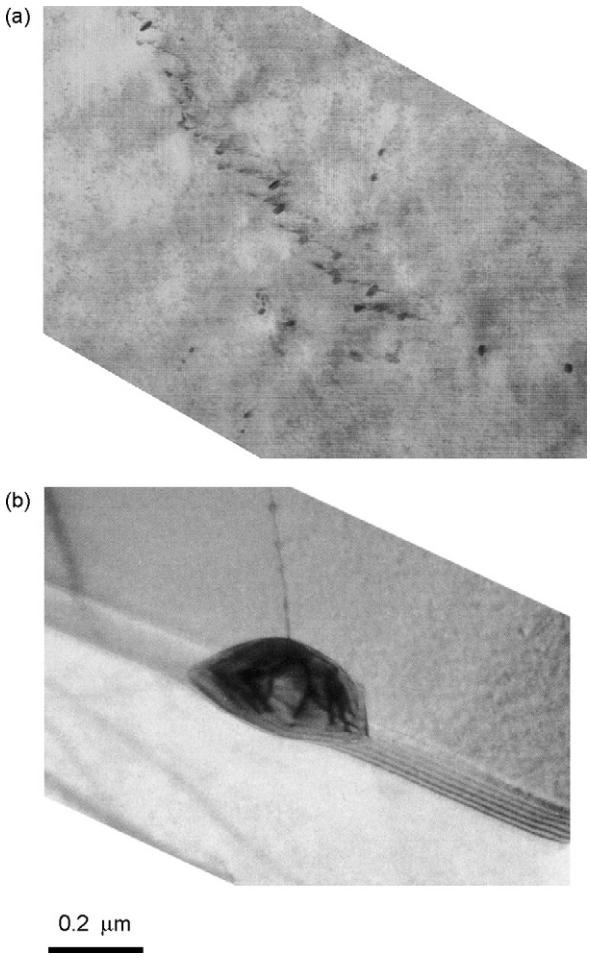

Fig. 4. TEM micrographs of (a) Cu particles on dislocations, $L = 0.1$ °C/s and (b) Cu particles on a grain boundary, $L = 0.02$ °C/s.

micrograph of Cu particles on dislocations (the dislocation density is $\sim 3 \times 10^{13}$ m^{-2} in this area) in the specimen cooled at $L = 0.1$ °C/s. These particles have presumably transformed to fcc (or 9R structure) and thus, started to elongate. This implies that the assumption of sphericity results in a crude estimate of volume fraction of particles at prolonged aging. Fig. 4b illustrates a micrograph of a Cu particle formed on the grain boundary. Whilst the matrix grain size was not measured for this specimen, the mean grain size was estimated to be ~50 μm from a previous study [2].

Three-dimensional (3D) APFIM analyses were conducted with a CAMECA optical tomographic atom probe (OTAP). They were performed under a vacuum of 10^{-8} Pa with a pulse fraction of 20%, a pulse repetition rate of 1 kHz and at a specimen temperature of 50 K. There was no difficulty to distinguish between iron and copper atoms since the mass-to-charge ratio of the former was mainly around 28 (they were actually Fe^{2+} ions), and the ratio of the latter was around 31.5 (Cu^{2+} ions), which was easily resolved by the instrument. The detection efficiency was assumed to be 50% and this was taken into account when the radius of a cluster was calculated from the number of detected ions. Fig. 5 illustrates a distribution of Cu atoms in the specimen cooled at $L = 0.1$ °C/s, where Fe atoms are not shown for clarity. Several Cu clusters are readily recognized as aggregates

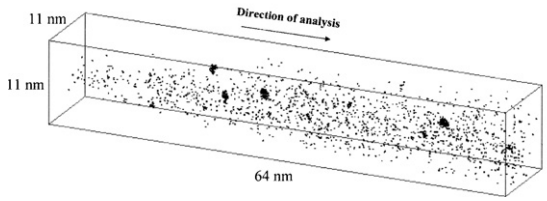

Fig. 5. APFIM mapping image illustrating Cu precipitates in a Fe–1.5Cu alloy continuously cooled at $L = 0.1\,^{\circ}C/s$.

of Cu atoms and an approximate size of the Cu clusters could be determined even with a naked eye. In order to locate Cu clusters systematically a sampling method with a specific concentration threshold was applied. The presence of Cu clusters were explored by moving the sampling volume of a diameter ranging from 1 to several nanometers in the whole data set, and if the Cu concentration in the volume was determined to be greater than 5 at.%, the sampling volume was recognized as a Cu cluster. The error range of particle number is possibly one order of magnitude.

4. Results and discussion

4.1. Particle size and number density in continuously cooled alloy

It is assumed in the calculation that the dislocation density of specimens re-heated to 830 °C, was $\rho \sim 10^{14}\ m^{-2}$ at the onset of continuous cooling. Figs. 6–9 show variations with temperature of the calculated nucleation rate, particle density, mean and critical radii of particles and mean Cu concentration in the matrix. It is seen immediately that the nucleation rate is quite sensitive to cooling rate (Fig. 6a–c). This is because at the slower cooling rate particles have time to grow and the supersaturation decreases faster (Fig. 9a–c). Nucleation occurred at a lower temperature at grain boundaries than in the matrix and at dislocations. This is due to our assumption that fcc particles with a larger nucleus/matrix interfacial energy are nucleated at grain boundaries.

In Fig. 8a–c the mean particle radius increases initially because of relatively high diffusivity at higher temperatures, whereas it decreases with decreasing temperature. This is primarily because coarsening occurs very slowly due to sluggish diffusivity at lower temperatures. Besides, the system continues to be supplied with new nuclei of smaller critical radius unless nucleation rate totally diminishes. These nuclei grow very slowly due to Gibbs–Thomson effect and low diffusivity. The calculated particle radii were considerably smaller than those observed, especially in Fig. 8b and c. Since the critical radius becomes smaller than the possible lower limit of detection by APFIM, the mean particle radius was calculated for particles greater than the minimum detectable size (≥0.5 nm). However, it was marginally greater than the mean size of all the particles, the difference between the two mean values being even smaller for particles on dislocations and almost null for grain boundaries.

It is seen in Fig. 7a–c that the calculated particle density depends on the cooling rate at early stages of precipitation,

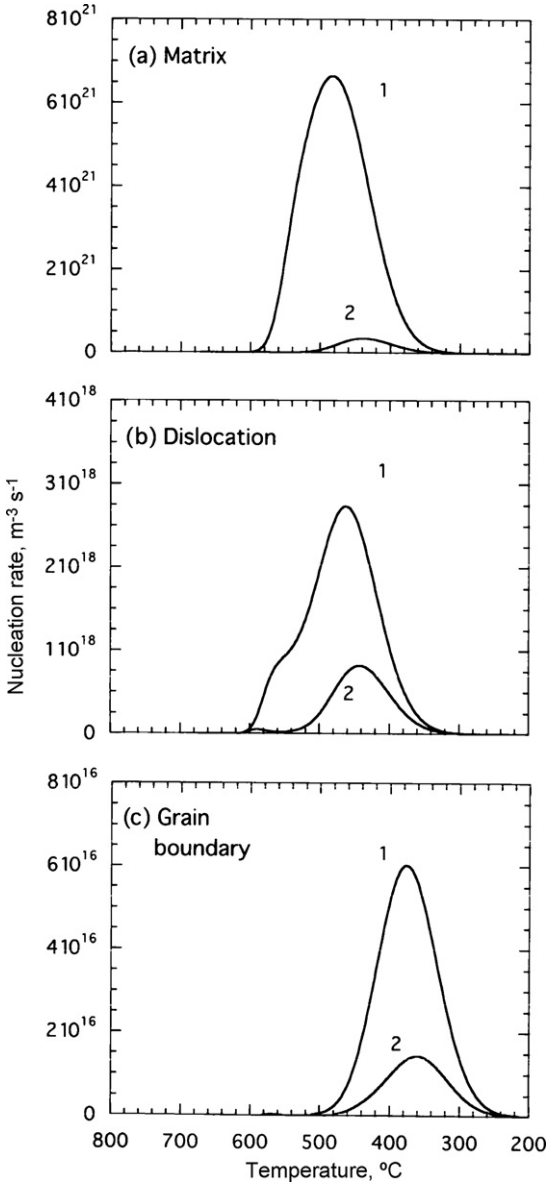

Fig. 6. Variation with temperature of calculated nucleation rate (a) in the matrix, (b) on dislocations, and (c) on grain boundaries in a continuously cooled Fe–1.5Cu alloy. The cooling rate is $L = 0.1$ (curves denoted 1) and $0.02\,^{\circ}C/s$ (curves 2).

whereas the difference is retained to room temperature only for particle density in the matrix. It seems to be odd that the particle numbers at the slower cooling rate are significantly greater initially whereas the nucleation rates appear to be smaller compared to those at the faster cooling rate (Fig. 6). This is an artifact caused by plotting in a linear- and log-scale. As shown in Fig. 10, the nucleation rates at initial stages are almost identical for the two cooling rates and thus, the particle numbers for the slow cooling rate become larger since the elapsed time is longer. It is noted that the calculated nucleation rate at $L = 0.02\,^{\circ}C/s$ has two peaks at ~600 and 540 °C during cooling. This is because fast growth of earlier nucleated particles deprives the matrix of driving force for nucleation and it rises again at lower temperatures.

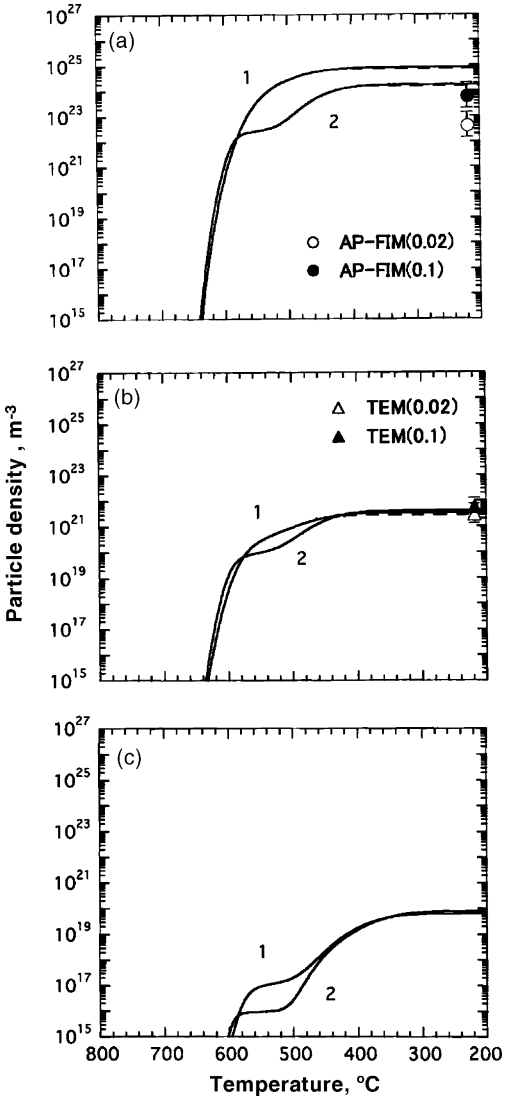

Fig. 7. Variation of particle density (a) in the matrix, (b) on dislocations, and (c) on grain boundaries, with temperature in a Fe–1.5Cu alloy calculated at $L = 0.1$ (curves 1) and 0.02 °C/s (curves 2). Dashed curves show variation of the density of particles greater than 0.5 nm, possible detection limit of APFIM.

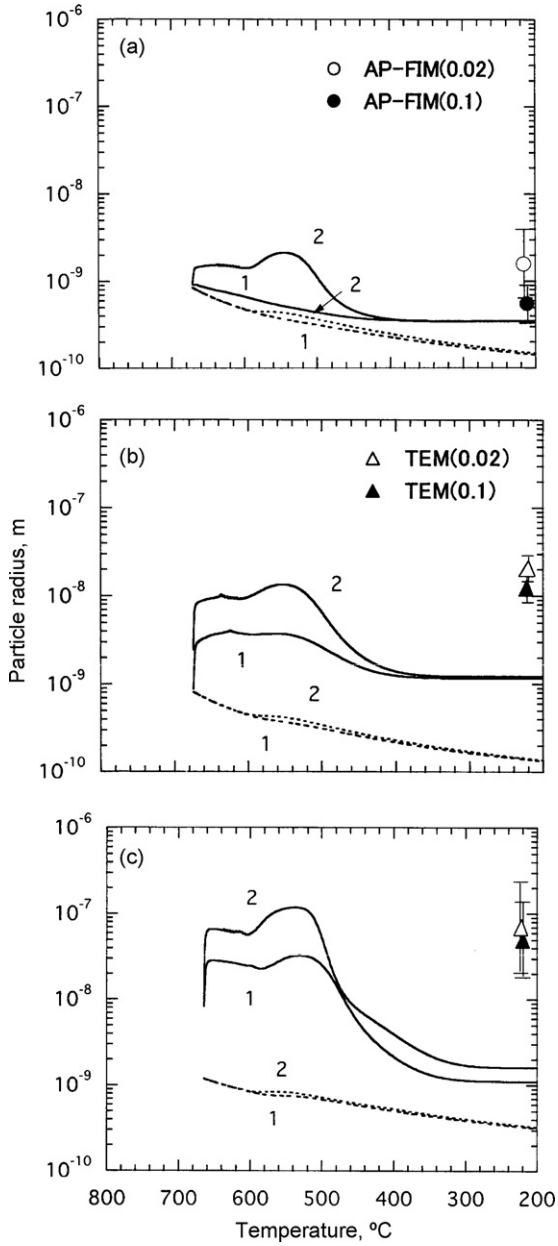

Fig. 8. Variation with temperature of calculated mean particle radius (solid curves) and critical radius (dotted curves) (a) in the matrix, (b) on dislocations, and (c) on grain boundaries in a Fe–1.5Cu alloy continuously cooled at $L = 0.1$ (curves 1) and 0.02 °C/s (curves 2).

Furthermore, the observed particle number in the matrix after cooling was more than one order of magnitude less than the calculated particle numbers. The calculated particle number is greater even when particles smaller than the detection limit were subtracted (dashed curves). The agreement between the observed and calculated particle numbers is apparently good on dislocations. The particle density on grain boundaries were not measured because of fewer areas of observation due to the relatively large grain size. It is noted that the particle density observed in the matrix is significantly smaller than calculation. This might be due to the large probe diameter ($\geq$1 nm). Alternatively, the assumption of constant particle/matrix interfacial energy in a wide temperature range might be responsible for these discrepancies because the interfacial energy tends to increase with lowering temperature due to the entropy term. The Cahn–Hilliard non-classical nucleation theory [2,28] possibly accounts better for the temperature dependence of the activation energy for nucleation.

Continuously cooled transformation (CCT) curves were calculated and are compared with time-temperature-transformation (TTT) curves in Fig. 11. As usually expected, the CCT curves lie to the right of the TTT curves above the nose temperature, whereas it is not the case below the nose temperature. This implies that Cu precipitation occurs faster by continuous cooling than by isothermal aging if the aging temperature is low. Physically this is because sub-critical nuclei have been formed at a higher temperature in continuous cooling and this is taken into account by Eq. (6) in the calculation. Aging of pre-strained alloys is actually performed at such a low temperature.

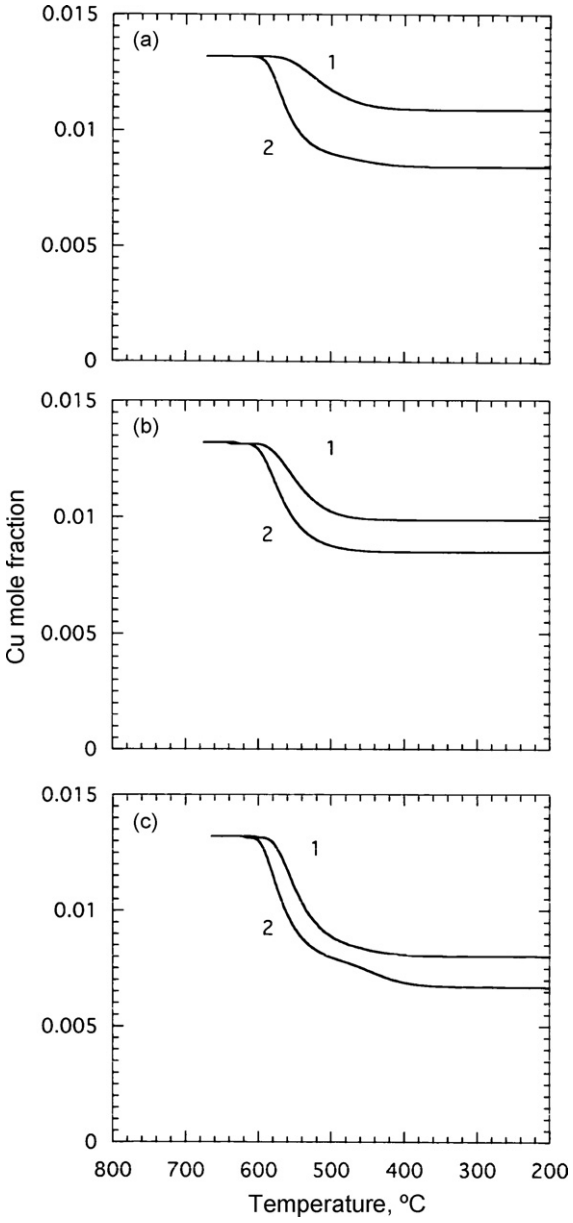

Fig. 9. Variation with temperature of solute concentration (a) in zone 1 (matrix), (b) in zone 2 (dislocation), and (c) in zone 3 (grain boundary) in a Fe–1.5Cu alloy calculated at $L = 0.1$ (curves 1) and 0.02 °C/s (curves 2).

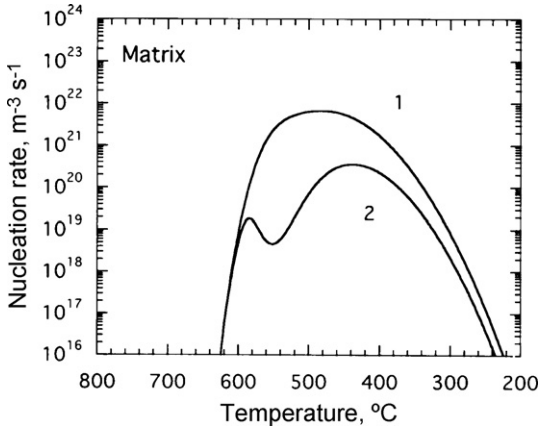

Fig. 10. Logarithmic plot of calculated nucleation rate in the matrix in Fig. 6a.

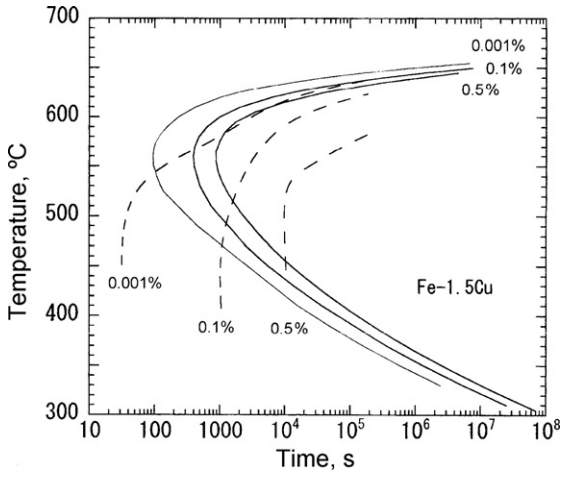

Fig. 11. Calculated CCT and TTT curves for Cu precipitation in the matrix in a Fe–1.5Cu alloy.

4.2. Nucleation, growth and dissolution of Cu particles during continuous heating

Simulations were conducted assuming that initially no Cu precipitates were present in the alloy. Fig. 12 shows variation with temperature of calculated nucleation rates in the alloy, having the same dislocation density ($\rho = 10^{14}\ m^{-2}$) and continuously heated at $L = 0.17$ °C/s. Nucleation began to occur at dislocations around 400 °C and somewhat below 500 °C in the matrix. As seen in Figs. 13 and 14, Cu particles nucleated in the matrix grew for some time, but soon began to decrease in volume fraction and totally disappeared at ~670 °C, i.e. 85 °C below the solvus of bcc Cu (755 °C). This is because the volume fraction of zone 3 of homogeneous nucleation decreases due to the expansion of solute-depleted zone around dislocations and grain boundaries. In other words, smaller particles in the matrix dissolve faster than those in the other zones in the global competition during coarsening. It can be shown that at a smaller dislocation density particles in the matrix remained up to a higher temperature, Unfortunately, direct experimental evidence for early dissolution of particles in the matrix is yet to be obtained.

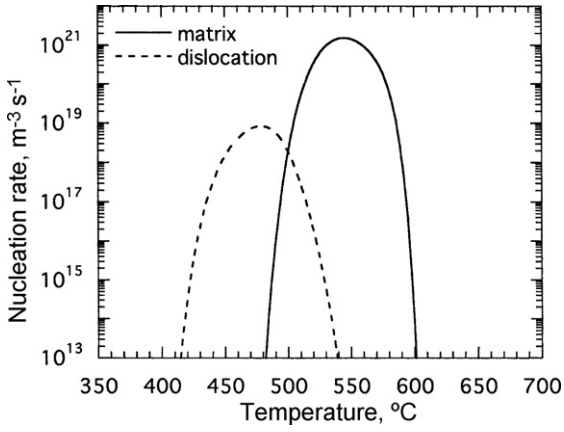

Fig. 12. Variation with temperature of calculated nucleation rate in the matrix (solid curve) and on dislocations (dashed curve) in a Fe–1.5Cu alloy continuously heated at $L = 0.17$ °C/s and $\rho = 10^{14}\ m^{-2}$.

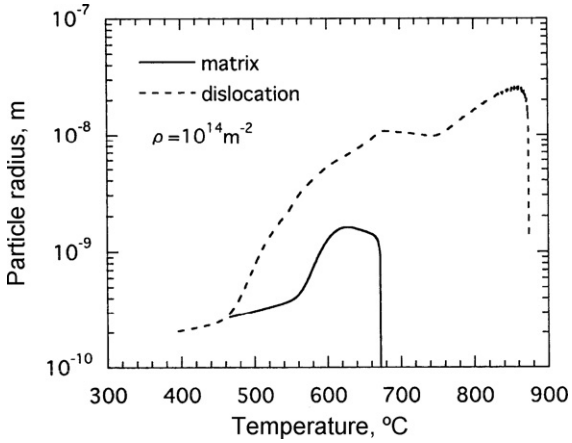

Fig. 13. Variation with temperature of calculated mean particle radius in the matrix (solid curve) and on dislocations (dashed curve) in a Fe–1.5Cu alloy continuously heated at $L = 0.17\,^{\circ}$C/s. The dislocation density is 10^{14} m^{-2}.

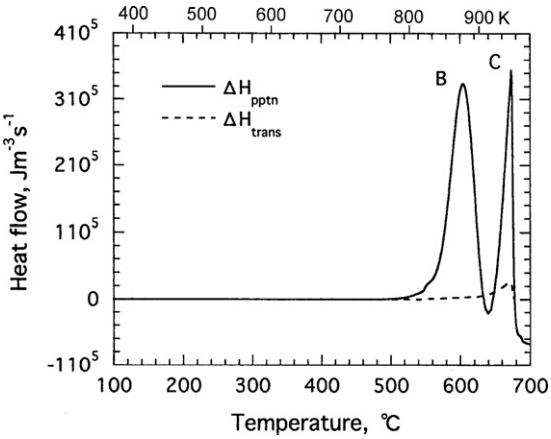

Fig. 15. Calculated heat evolution of a Fe–1.5Cu alloy during continuous heating at $L = 0.17\,^{\circ}$C/s. The solid curve is the heat generated due to precipitation and the dashed curve, due to structural transformation.

Maruyama et al. [29] studied Cu precipitation in ferritic and martensitic steels by differential scanning calorimetry (DSC). They observed three exothermic peaks that were attributed to the formation of Cu nuclei (∼330 °C in the deformed ferritic steel), Cu diffusion in the bcc Fe matrix (∼560 °C) and structural transformation from bcc to fcc Cu particles (∼610 °C), see Fig. 9 of Ref. [27]. In comparison with these observations, first, the 1st broad peak did not appear in this simulation. This is probably because the formation of sub-critical solute clusters was not considered in this modeling. Second, the heat evolution was calculated from the latent heat of structural transformation of Cu particles ($H_{\mathrm{trans}}^{\mathrm{bcc}\rightarrow\mathrm{fcc}} = -4017 + 1.255T$ J/mol [30]) and the heat of dissolution of Cu particles ($H_{\mathrm{sol}}^{\varepsilon\mathrm{Cu}} = 84.4$ kJ/mol [31]). It is seen in Figs. 14 and 15 that the calculated peaks at ∼600 °C and ∼670 °C are caused by rapid increase in the volume of bcc and fcc particles, respectively. It is tentatively proposed that they correspond to the 2nd and 3rd peaks observed in DSC analysis, which are denoted peaks B and C, respectively. Since $\Delta H_{\mathrm{trans}}$, heat evolved by transformation (dashed curve), is much smaller than ΔH_{pptn}, heat evolved by precipitation of bcc or fcc particles (solid curve), it is likely that the observed 3rd peak is caused not only by structural transformation, but also by rapid growth of transformed particles. The calculated peak temperatures are considerably different from those of DSC analysis. This is probably because the former temperatures vary quite sensitively with the assumed dislocation density and diffusivities as well.

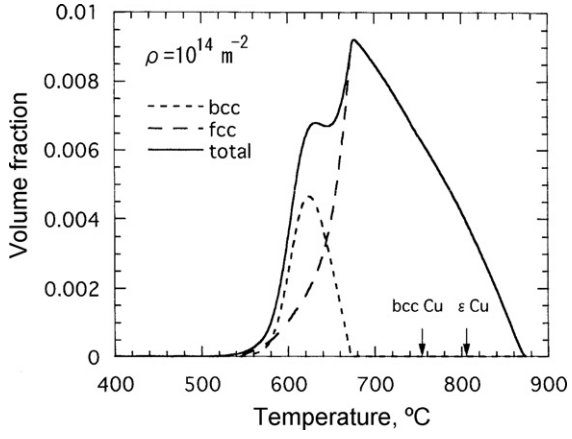

Fig. 14. Variation with temperature of volume fraction of bcc (dashed curve), fcc (long-dashed curve) and the sum of bcc and fcc Cu particles (solid curve) calculated at $L = 0.17\,^{\circ}$C/s and $\rho = 10^{14}$ m^{-2}. The arrows indicate the solvus temperature of bcc and fcc Cu.

5. Summary

Cu precipitation in a bcc Fe–1.5Cu alloy during continuous cooling and heating was simulated taking into account competitive nucleation at grain boundaries, dislocations and in the matrix, and structural transformation of Cu particles. The temporal evolution of nucleation rate, particle density, mean particle size and size distribution and supersaturation in the matrix was simulated assuming that the system was composed of more than one zone, i.e. solute-depleted zones associated with heterogeneous nucleation sites and the matrix. Nucleation was assumed to occur as bcc Cu in the matrix and at dislocations, and as fcc Cu at grain boundaries.

Whereas the growth and coarsening rates of Cu particles diminished rapidly in continuous cooling, nucleation continued to occur at lower temperatures because the increase in the amount of undercooling overrode the decrease in diffusivity. Calculated particle sizes were considerably smaller than observed ones whereas calculated particle numbers tend to be greater than observations. It is tentatively proposed that a significant proportion of smaller particles were not duly counted, albeit a further investigation that incorporates the temperature dependence of the particle/matrix interfacial energy is necessary. One can expedite Cu precipitation by continuous cooling rather than low temperature aging because sub-critical Cu clusters are formed readily at higher temperatures in the course of cooling.

Simulation results of Cu precipitation in continuous heating indicated the existence of two exothermic peaks that were comparable to those reported by a DSC (differential scanning calorimetry) study [29]. The peaks can be attributed to the nucleation and growth of bcc Cu and growth of fcc particles, respectively, although the simulated peak temperature depends

considerably on the assumed dislocation density and diffusivities controlling the precipitation at heterogeneous sites.

Acknowledgements

This research was conducted as a part of the research activities of the Ferrous and Computational Materials Science Consortia of the Nanometal Project under the auspices of The Japan Research and Development Center for Metals, Tokyo.

References

[1] R. Kampmann, R. Wagner, in: P. Hassen, V. Gerold, R. Wagner, M.F. Ashby (Eds.), Decomposition of Alloys; The Early Stages, Pergamon Press, Oxford, 1984, p. 91.
[2] C. Zhang, M. Enomoto, T. Yamashita, N. Sano, Metall. Mater. Trans. A 35A (2004) 1263.
[3] J.B. Yang, M. Enomoto, ISIJ Int. 45 (2005) 1335.
[4] J.B. Yang, M. Enomoto, C. Zhang, Mater. Sci. Eng. A 422 (2006) 232.
[5] F. Soisson, A. Barbu, G. Martin, Acta Mater. 44 (1996) 3789.
[6] A. Cerezo, S. Hirosawa, I. Rozdilsky, G.D.W. Smith, Philos. Trans. R. Soc. (London) A 316 (2003) 463.
[7] P.R. Monasterio, B.D. Wirth, G.R. Odette, J. Nucl. Mater. 361 (2007) 127.
[8] M.H. Mathon, A. Barbu, F. Dunstetter, F. Maury, N. Lorenzelli, C.H. de Novion, J. Nucl. Mater. 245 (1997) 224.
[9] O.R. Myhr, Ø. Grong, Acta Mater. 48 (2000) 1605.
[10] M. Nicholas, A. Deschamps, Acta Mater. 51 (2003) 6077.
[11] H.I. Aaronson, J.K. Lee, in: H.I. Aaronson (Ed.), Lectures on the Theory of Phase Transformations, Second ed., TMS-AIME, Warrendale, PA, 2000, p. 165.
[12] B. Jansson, M. Schalin, M. Selleby, B. Sundman, Mater. Soc. CIM Quebec (1993) 57.
[13] C.C. Dollins, Acta Metall. 18 (1970) 1209.
[14] F.C. Larche, Solid State Phenomena 35/36 (1994) 173.
[15] G.J. Ackland, D.J. Bacon, A.F. Calder, T. Harry, Philos. Mag. A 75 (1997) 713.
[16] C. Domain, C.S. Becquart, Phys. Rev. B 65 (2001) 1.
[17] Z.G. Yang, M. Enomoto, Mater. Sci. Eng. A 332 (2002) 184.
[18] Y. Le Bauer, Acta Mater. 49 (2001) 2661.
[19] N.A. Gjostein, H.A. Domian, H.I. Aaronson, E. Eichen, Acta Metall. 14 (1966) 1637.
[20] J.W. Cahn, Acta Metall. 4 (1956) 449.
[21] J.D. Robson, M.J. Jones, P.B. Prangnell, Acta Mater. 51 (2003) 1453.
[22] M. Enomoto, N. Nojiri, Scripta Mater. 36 (1997) 625.
[23] H.B. Aaron, H.I. Aaronson, Acta Metall. 16 (1968) 789.
[24] J. Fridberg, L.-E. Torndahl, M. Hillert, Jernkont. Ann. 153 (1969) 263.
[25] N.L. Peterson, Grain-boundary Structure and Kinetics, ASM, Metals Park, 1980, p. 209.
[26] P.J. Othen, M.L. Jenkins, G.D.W. Smith, Philos. Mag. A 70 (1994) 1.
[27] R. Monzen, M.L. Jenkins, A.P. Sutton, Philos. Mag. A 80 (2000) 711.
[28] J.W. Cahn, J.E. Hilliard, J. Chem. Phys. 31 (1959) 688.
[29] N. Maruyama, M. Sugiyama, T. Hara, H. Tamehiro, Mater. Trans. JIM 40 (1999) 268.
[30] A.T. Dinsdale, CALPHAD 15 (1991) 317.
[31] L.J. Swartzendruber, in: H. Okamoto (Ed.), Phase Diagrams of Binary Iron Alloys, ASM International, Metals Park, OH, 1993, p. 131.